Phase stability of decomposed Ni-Al alloys under ion irradiation

G. Schmitz* and J. C. Ewert
Institut für Materialphysik, Univ. Göttingen, Hospitalstr. 3-7, D-37073 Göttingen, Germany

F. Harbsmeier and M. Uhrmacher
II. Physikalisches Institut, Univ. Göttingen, Bunsenstr. 7-9, D-37073 Göttingen, Germany

F. Haider
Lehrstuhl für Experimentalphysik I, Univ. Augsburg, Memminger Str. 6, D-86159 Augsburg, Germany
(Received 15 November 2000; revised manuscript received 19 March 2001; published 23 May 2001)

The disordering of a decomposed Ni-12 at. %-Al alloy under irradiation with 300-keV Ni^+ ions is studied in direct comparison to homogeneous Ni_3Al at various temperatures. For that, the degree of long-range order is quantitatively determined by electron diffractometry. Heterogeneous alloys disorder significantly faster than the homogeneous intermetallic. In addition, their disordering rate depends on the precipitate size of the microstructure. At 823 K a steady state with an intermediate degree of order is reached. The experimental results are compared with model calculation based on a Cahn-Hilliard-type continuum model. At higher temperatures the model yields a correct description of the experiments. However, discrepancies at room temperature suggest a direct coupling of local composition and degree of order during the collision cascade. This interpretation is further supported by Monte Carlo simulations of overlapping cascade events.

DOI: 10.1103/PhysRevB.63.224113 PACS number(s): 61.80.Jh, 64.60.Cn, 61.14.−x, 81.05.Bx

I. INTRODUCTION

Phase stability and microstructural evolution of ballistically forced alloys are a long term interest of material physics. Whenever a system is driven from thermodynamic equilibrium, e.g., by irradiation with energetic particles, a variety of different phenomena may occur depending sensitively on the actual experimental condition.[1] In this case, kinetic considerations become especially important to predict the evolution and eventual steady states of the system. Advanced theoretical concepts are required to develop a sufficient physical description.[2,3]

Since the mechanical properties of structural materials are often tailored by optimizing a heterogeneous microstructure, it is not surprising that the behavior of precipitates in irradiated materials has been investigated already for several decades.[4] However, the physically very fascinating and technologically important case of ordered precipitates embedded in a disordered matrix attracted systematic attention only at the end of the last century, after a sufficient understanding of homogeneous intermetallics had been achieved.[5] In this case, the interplay between order and local composition raises interesting questions. Which of the two processes, dissolution or disordering, proceeds faster? Does disordering destabilize the precipitates, so that the ballistic mixing is in addition accelerated by thermodynamic forces? On the other hand, the experimental study of these phenomena is a challenging problem as composition and order of small precipitates of nm size must be determined.

For our study, we chose the binary system NiAl since this system shows a pretty high-order contrast in electron diffractograms. Furthermore, it forms the base of many technological important superalloys so that reliable thermodynamic and kinetic data are available. The disordering of homogeneous Ni_3Al by ball milling[6–9] or electron irradiation[10–12] has already been investigated intensively. Fewer studies on ion-induced disordering of the homogeneous material are reported.[13,14] Owing to the very heterogeneous damage produced by localized cascade events, one may consider irradiation with heavy ions as a considerably more complex case than irradiation with electrons. Nevertheless, the introduced damage can still be quantified in terms of displacements per atom by well established methods[15,16] so that the competition between ballistic and thermal jumps can be investigated quantitatively. In contrast to electron irradiation, with ion irradiation complete disorder of the alloy is achieved still above room temperature, which allows us to perform experiments at convenient temperatures.

Ordered precipitates have been investigated already in two experimental studies on a Ni-based superalloy which is structurally very similar to binary NiAl. The chemical dissolution of precipitates was determined by atom probe analysis.[17] Indeed, characteristic changes of the composition gradient at the particle interfaces with increasing temperature were found which have been interpreted by Martin *et al.*[5] as evidence supporting their theoretical result of two different temperature regimes regarding the sequence of disordering and dissolution. However, one must not overlook that the order structure and in consequence the type of the equilibrium phase transition are quite different in the experimental and theoretical studies. Bourdeau *et al.*[18] observed the disordering by electron diffractometry. Because of the weak order contrast of their multicomponent alloy, the order degree could be determined only in an at most semiquantitative manner.

In this work we present a study on ion-induced disordering of decomposed binary NiAl alloys by quantitative electron diffractometry. The experimental data are interpreted in terms of actual theoretical concepts on the phase stability under irradiation. A direct comparison of decomposed alloys

to homogeneous Ni_3Al reveals that intracascade effects must be taken into account to understand the kinetics. The paper is organized as follows: After a short description of the experimental methods, experimental results on disordering of decomposed alloys as well as homogeneous Ni_3Al are presented. Then, a kinetic continuum model based on Cahn-Hilliard-type equations is derived in order to give a first interpretation of the data. It turns out that this model correctly describes the behavior at elevated temperatures while it is insufficient to explain the disordering of heterogeneous alloys at room temperature. In a further section, we show that this shortcoming is due to the neglect of intracascade dynamics. A kinetic Monte Carlo model is proposed, taking into account a partial relaxation of order inside the cascade core, which is indeed sufficient to explain the observed faster disordering of small precipitates. In a final discussion assumptions underlying the models and consequences of the limited experimental accuracy are considered.

II. EXPERIMENTAL METHODS

Two different NiAl alloys with nominal 12 and 25 at. % Al were prepared from Al and Ni of 99.999% purity by inductance melting under Ar atmosphere. The compositions were proven to be 11.5 ± 1 and 24 ± 1 at. % by microprobe analysis. Both alloys were homogenized at 1100 °C for seven days. In the Al-poor alloy, a heterogeneous microstructure was formed consisting of spherical Ni_3Al precipitates embedded in a disordered matrix of about 10.5 at. % Al. Aging at 600 °C for 3 and 24 h yielded particle size distributions of 2.6 ± 0.6 and 4.6 ± 0.9 nm mean radius, respectively. Cylindrical discs of 2.3 mm diameter and 0.1 mm thickness were cut by spark erosion and thinned to electron transparency by the usual jet polishing technique using an electrolyte of 95 vol% acetic and 5 vol% perchloric acid at 15 °C.

Thinned specimens were irradiated with 300-keV $^{58}Ni^+$ ions using the implanter IONAS (Refs. 19 and 20) in Göttingen. Besides irradiation at room temperature, a heated target stage allowed irradiation also at 450 and 550 °C. The temperature stability of the stage amounts to ±5 °C. The irradiation temperature is reached with a heating rate of 20 K/s. Subsequent to irradiation, specimens were quenched to room temperature with a cooling rate of 2 K/s. In order to calibrate the irradiation damage, the ballistic collisions were simulated applying the TRIM program.[15] A penetration depth of about 100 nm and a thickness averaged displacement cross section of 1.65×10^{-19} m^2 is predicted. Using beam currents between 10 and 100 nA/cm^2 corresponding to a damage rate of 10^{-4}–10^{-3} dpa/s, the specimens were irradiated to maximum doses of 5 dpa. During the irradiation, the ion beam was scanned across the specimen ensuring a laterally homogeneous damage distribution.

Owing to the very limited penetration depth of the ions, the damaged volume inside the specimens is rather small. Therefore x-ray diffractometry can hardly be used to determine long-range order parameters. Instead, we investigated the damaged zone directly with electron microscopy. The degree of order is determined from electron-diffraction intensities, where dynamical scattering has to be taken into account. In order to get reproducible results, the specimens are always oriented in a {112} zone axis beam condition and a thickness averaging is performed along the wedge-shaped specimens. Details of the quantitative evaluation method are described in a recent paper[21] on thermal reordering of Ni_3Al.

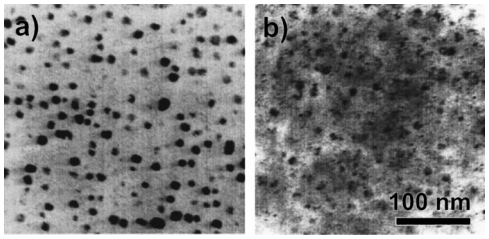

FIG. 1. Dark field images of Ni-12 at. %-Al using the (100) reflection (a) after 24 h aging at 873 K, (b) after an additional irradiation treatment at room temperature to 0.05 dpa.

III. EXPERIMENTAL OBSERVATIONS

Irradiation at room temperature with dose rates between 10^{-4} dpa/s and 10^{-3} dpa/s completely destroys the long-range order (LRO) in homogeneous Ni_3Al and in decomposed alloys as well. In the latter case, besides the homogeneous disordering of the Ni_3Al phase inside the precipitates, the interfaces become rough and the precipitates start to shrink already at very low doses, as shown in Fig. 1. On the other hand, no indications for an amorphization are observed in the diffraction patterns. The development of LRO is shown in Fig. 2 for three different initial microstructures. In each case, the degree of order was normalized to that determined before irradiation taking into account the smaller ordered volume fraction of the Al-poor alloys. Within the experimental accuracy, the behavior of homogeneous Ni_3Al is well described by a simple exponential decay,

$$S(\Phi)=S_0\cdot e^{-\epsilon\Phi}, \tag{1}$$

with a disordering efficiency of $\epsilon=16\pm0.5$ dpa^{-1}. No finite rest order is observed in the high dose limit. Remarkably, the decomposed microstructures disorder much faster than the

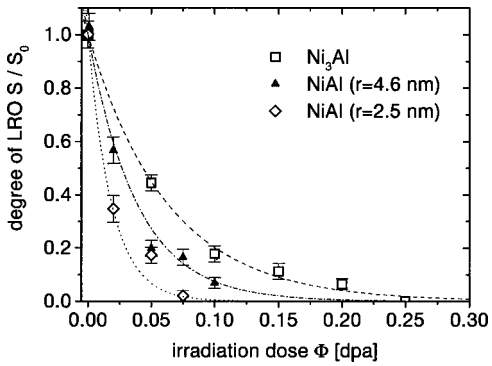

FIG. 2. Development of long-range order in Ni_3Al and decomposed alloys (Ni-12 at. %-Al) during irradiation at room temperature ($\dot{\Phi}=10^{-4}$ dpa/s). Solid and dashed lines represent exponential decays according to Eq. (1).

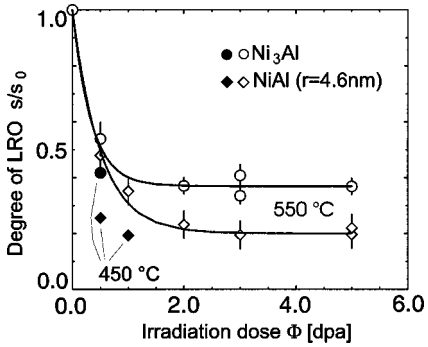

FIG. 3. LRO parameter during irradiation at elevated temperatures in Ni_3Al and in decomposed alloys (Ni-12 at. %-Al) with particles of 5 nm radius ($\dot{\Phi}=10^{-3}$ dpa/s). At 823 K, a steady state is established in both microstructures as indicated by the solid lines.

homogeneous system and, furthermore, the disordering efficiency increases with decreasing particle size. Assuming an exponential dependence also for the heterogeneous systems, disordering efficiencies may be quantified to $\epsilon=26$ dpa^{-1} and $\epsilon=54$ dpa^{-1} for particles with 4.6 and 2.6 nm mean radius, respectively. The disordering kinetics slows down significantly with increasing irradiation temperatures, see the data for 723 and 823 K in Fig. 3. In this case a dose rate of 10^{-3} dpa/s was chosen, to allow the efficient competition between thermal and ballistic jumps. The data at 823 K strongly suggest the existence of a steady state in the homogeneous as well as in the decomposed microstructure with 4.6-nm particle radius. However, the stationary degree of order of the decomposed specimens is only about half of that observed for homogeneous Ni_3Al. The development of the particle size distribution in a decomposed system is shown in Fig. 4. Starting from the initial mean radius of 4.6 nm, the particles shrink during the irradiation treatment until a mean radius of 2.0 nm is reached in the steady state.

IV. COMPARISON WITH A CONTINUUM APPROACH

In the case of the heterogeneous system, the interplay between order and local composition essentially controls the dissolution of the precipitates and thus the average disordering kinetics which is determined by the experiments. Comparing the behavior of the heterogeneous system to homogeneous Ni_3Al may elucidate characteristic features of the interaction between order and alloy composition. As the most striking result of this comparison, our experiments demonstrate that precipitates disorder significantly faster

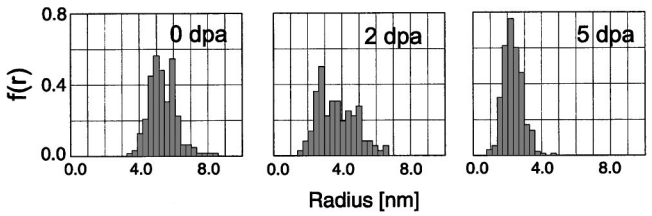

FIG. 4. Size distributions of ordered precipitates in Ni-12 at. %-Al during irradiation at 823 K using a dose rate of $\dot{\Phi}=10^{-3}$ dpa/s.

than homogeneous Ni_3Al. In a preliminary discussion of part of the presented data[22] we argued that this effect is due to ion mixing which takes place in addition to ion-induced disordering. As soon as the local composition at the particle's interface falls below a critical limit of $c^*=0.17$, the ordered phase becomes instable and disorders spontaneously. However, a rather large ion-mixing efficiency of $\kappa=14$ nm^2/dpa is necessary to obtain quantitative agreement with the experimental data. In order to further test this interpretation, the disordering kinetics must be discussed in more detail.

Martin and co-workers developed a general scheme based on a master equation for the different configuration probabilities in order to describe systems under external ballistic forcing. In the case of $B2$ ordered precipitates, they predicted two temperature regimes regarding the sequence of disordering and dissolution.[5] But no explicit solution for precipitates of $L1_2$ structure, characterized by a phase transition of first order, was given. Therefore, to get an analytical description of the interaction between composition and order, we follow an earlier suggestion of Martin[23] to formulate kinetic continuum equations. Matsumura *et al.*[24] were already using continuum equations to describe Ni based superalloys under ion irradiation. However, their kinetic equations contain several temperature-dependent parameters, necessary to model the thermodynamics of the NiAl system, which are not *a priori* known. In the following we reformulate similar equations using a thermodynamic model appropriate to the $L1_2$ order transition to obtain a simple analytical model with a minimum set of free parameters. Our aim is to test qualitatively whether the observed steady state and the faster disordering of precipitates may be understood by the continuum approach rather than to give a quantitative exact description.

Regarding the heterogeneous system, composition and LRO parameters may no longer be treated as position independent. Instead, they have to be introduced as field variables, which are determined by a local average on a medium-sized scale of several lattice constants. Allowing for deviations from stoichiometry, we define the LRO parameter by

$$s := \frac{1}{3}\left(\frac{c_\alpha}{c}-1\right), \tag{2}$$

where c and c_α denotes the local Al concentration averaged on all sublattices and the Al concentration of the ''corner'' sublattice which is occupied predominantly by Al atoms in the $L1_2$ structure. The coupling between the composition and LRO fields is described to first approximation by the Gibbs free energy, although strictly the occupancy of the different configurations in thermal equilibrium is disturbed in the driven system. The most simple representation of evolutionary equations for order and composition is then given by

$$\frac{\partial c}{\partial t}=\kappa\dot{\Phi}\nabla^2 c+L(T,\dot{\Phi})\nabla^2\frac{\partial f(c,s,T)}{\partial c}-HL(T,\dot{\Phi})\nabla^4 c, \tag{3}$$

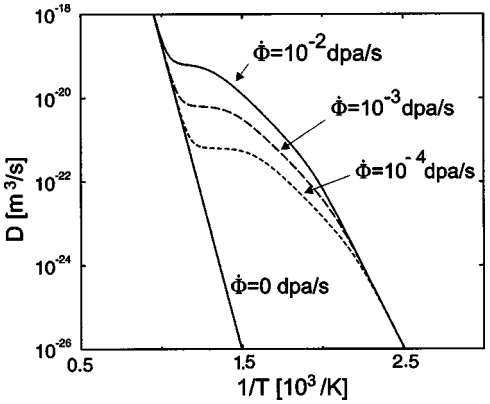

FIG. 5. Diffusion coefficient for the kinetic calculations presented in Sec. IV.

$$\frac{\partial s}{\partial t} = -\epsilon\dot{\Phi}s - M(T,\dot{\Phi})\frac{\partial f(c,s,T)}{\partial s}. \tag{4}$$

In the order of their appearance, the terms on the right-hand side describe the ballistic mixing or disordering, their thermal relaxation and finally, in the case of the composition field, interfacial contributions. κ, T, and H are mixing efficiency, temperature, and gradient energy coefficient, respectively. In general, also the kinetic equation for the order parameter should contain a gradient energy term taking into account the contribution of domain boundaries. However, a correct concept then requires the definition of the order parameter as a vector variable of three independent components, as three out of four sublattices may be occupied independently. Thus two further kinetic equations would have to be introduced. In order to avoid such complexity, this gradient term is neglected. Probably this simplification will not cause large errors as the calculated structures do not contain any antiphase boundary.

The mobility L is connected to the diffusion coefficient by the Einstein relation, $L=c(1-c)D/(kT)$. For the sake of simplicity, the variation of L with composition is neglected as the local composition varies only between about 10 and 25 at. %. However, the enhancement of the diffusion by irradiation induced vacancies may have an important effect. A quantitative estimate is obtained by standard rate equations.[25] The temperature dependence of the diffusion coefficient, which is used to integrate the kinetic equations, is shown in Fig. 5. Details of the calculation of point defect supersaturation and necessary parameters may be found in Ref. 26. As diffusion and ordering are based on the same microscopic mechanism, the mobility coefficients of mixing and ordering are interconnected. By mean-field considerations as presented in the Appendix, we found $M=16L/(3\,c^2a_0^2)$, where a_0 denotes the cubic lattice constant.

Matsumura and co-workers used a Ginzburg-Landau representation of the thermodynamic potential f in their kinetic approach to the NiAl system. As this potential was originally derived for the tricritical Fe-Al system, it does not yield a topologically correct description of the NiAl phase diagram.

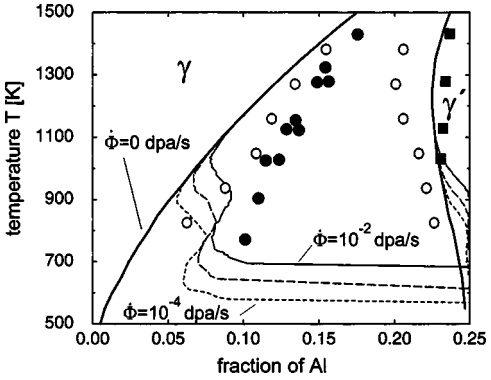

FIG. 6. Phase diagram between the terminating Ni phase and ordered Ni_3Al. The equilibrium phase boundaries ($\dot{\Phi}=0$ dpa/s) were calculated using Eq. (5). In the driven cases, steady-state boundaries were calculated using the generalized potential defined in Eq. (7). For comparison experimental data points Ref. 40 (filled circles) and the phase boundaries of the Monte Carlo model (open circles) are shown.

Instead, we prefer a mean-field expression introduced by Khachaturyan[27] to describe the transition between disordered AlLi and $L1_2$ ordered Al_3Li,

$$\begin{aligned} f(c,s,T) = {} & N/2c^2(V_0+3V_1s^2) + Nk_BT/4\{c(1+3s)\ln[c(1 \\ & +3s)] + [1-c(1+3s)]\ln[1-c(1+3s)]\} \\ & + 3Nk_BT/4\{c(1-s)\ln[c(1-s)] \\ & + [1-c(1-s)]\ln[1-c(1-s)]\}. \end{aligned} \tag{5}$$

This free-energy representation requires only two temperature-independent parameters V_0 and V_1 representing the Fourier components of the interaction potential to the spatial frequencies k_{000} and k_{001}. As these parameters have a clear physical meaning, an extrapolation to nonequilibrium conditions probably yields still reasonable results. In a qualitative sense, the phase diagram is predicted correctly by Eq. (5) if V_0 and V_1 are adjusted to $4500\ \mathrm{K}k_B$ and $-8300\ \mathrm{K}k_B$, respectively. However, the width of the phase fields is underestimated at low temperatures, see Fig. 6. After defining the thermodynamic potential, the gradient energy coefficient in Eq. (3) is adjusted to $H=256\ \mathrm{nm^2\,J/mol}$ in order to reproduce the experimental interfacial energy[28] of $14\ \mathrm{mJ/m^2}$.

The presented kinetic model allows us to predict the development of homogeneous as well as heterogeneous systems by simply integrating Eqs. (3) and (4). However, a first guess about the kinetics is already obtained when possible steady states are considered. In the case of a homogeneous phase with fixed composition, steady-state degrees of order s^* are obtained regarding $\partial s/\partial t(s^*)=0$. In addition, the conditions of stability $\partial s/\partial t(s^*-\epsilon)>0$ and $\partial s/\partial t(s^*+\epsilon)<0$ must hold. The resulting steady-state order parameter of homogeneous Ni_3Al is plotted versus the temperature in Fig. 7 for several dose rates. The equilibrium curve ($\dot{\Phi}=0$) reproduces the temperature dependence well known for a phase transition of first order, distinguished by a discontinu-

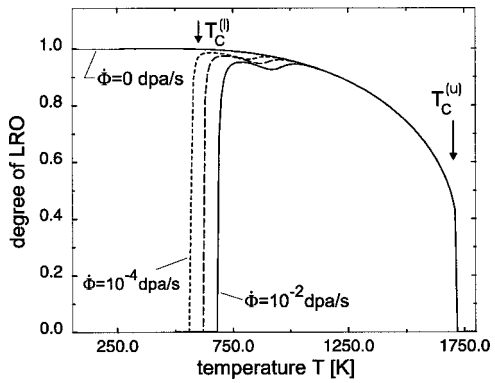

FIG. 7. Degree of order of stoichiometric Ni_3Al in the steady state of Eq. (4).

ity at an upper critical temperature. By irradiation, a second, lower critical temperature is established, below which the LRO is destroyed. As the steady-state is controlled by the competition between thermal and ballistic atomic jumps, this lower critical temperature depends significantly on the dose rate. By contrast, at the upper critical temperature, thermal jumps dominate the kinetics. Thus the phase stability is almost not influenced by irradiation, if experimental dose rates are considered.

For heterogeneous systems, a phase diagram describing the existence range of the ordered and disordered phases is necessary to understand the experiments. Neglecting interfacial contributions, as is usually done in equilibrium phase diagrams, we obtain for the steady state of Eq. (3)

$$\frac{\partial c}{\partial t}=0=\nabla^2\left(\gamma c+\frac{\partial f}{\partial c}\right)=\nabla^2\left(\frac{\partial \tilde{f}}{\partial c}\right). \tag{6}$$

The parameter $\gamma=\kappa\dot{\Phi}/L(T,\dot{\Phi})$ describes the strength of the external forcing, i.e., the number of ballistic displacements relative to the thermal ones. According to Eq. (6), the compositions at the phase boundaries may be determined by the common tangent construction to the modified potential

$$\tilde{f}(T,c,s,\dot{\Phi}):=f(T,c,s)-\frac{1}{2}\gamma(\dot{\phi})\cdot(1-c)c. \tag{7}$$

Phase boundaries calculated this way for systems under external forcing are included in Fig. 6. Below the lower critical temperature, where the ordered phase becomes unstable, the two-phase region disappears and the system becomes completely miscible. Between 600 and 1000 K, where irradiation enhanced diffusion turns out to be most efficient, the solubility of the terminating Ni phase is significantly increased by the irradiation. At high temperatures above 1000 K, the equilibrium remains nearly undisturbed similar, as already noticed, to the order parameter of the homogeneous system.

The temporal evolution of ordered precipitates is simulated within a cell model applying periodic boundary conditions. The calculations were restricted to a one-dimensional geometry to reduce the computational effort. Compared to a real three-dimensional process this simplification will only retard the mixing kinetics[29] and somewhat modify the volume fractions of the phases. Thus it is assumed that the main characteristics of the process are still described correctly. Similar to the experiment, equilibrium between the particle and surrounding matrix is established at 823 K before introducing the external forcing. This way, the deviation from the experimental phase diagram is naturally taken into account. The initial matrix composition before irradiation amounts to about 4.5 at. %. The total Al content is adjusted by the cell size to about 10 at. %, somewhat smaller than the experimental one to correct for the reduced matrix solubility.

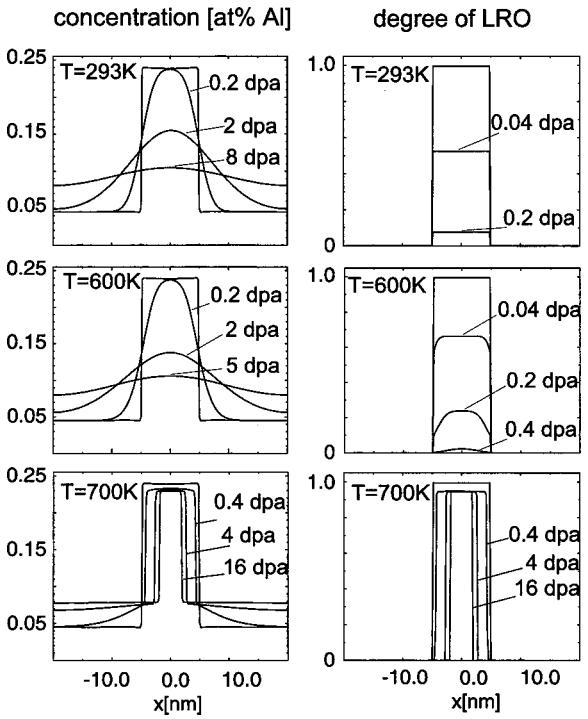

FIG. 8. Calculated development of composition and LRO profiles across a precipitate at three different irradiation temperatures, $\kappa=14$ nm^2/dpa, $\epsilon=16$/dpa, $\dot{\Phi}=10^{-3}$ dpa/s. The average composition of the cell amounts to 9.4 at. %.

Simulated composition and LRO profiles across a particle of 5 nm radius are presented in Fig. 8. Three different temperatures are selected. The room-temperature calculation corresponds to the experimental data in Fig. 2. Further temperatures are chosen near to the lower critical temperature of the steady-state phase diagram, 600 K just below and 700 K above the phase boundary inside the two-phase region. Therefore at the latter temperature a heterogeneous two-phase system is stabilized in the steady state. In this case, the thermal mobility is sufficient to establish a local equilibrium at the interfaces as indicated by rather steep gradients of order and composition profiles. Inside the precipitates a degree of order similar to that calculated for homogeneous Ni_3Al is quickly obtained. During further irradiation, the Al content of the matrix increases slowly by Al diffusion from the particles towards the matrix until the irradiation enhanced solubility limit is reached. In consequence, the average order of the decomposed system in the steady-state is determined by two effects. First, the order of the precipitate phase itself is reduced. In addition, the volume fraction of the ordered phase gets decreased by particle shrinkage which

explains the smaller degree of order in the steady state of the decomposed system in agreement with our experimental results.

Below the lower critical temperature, the precipitates are dissolved as expected from the phase diagram. Disordering proceeds significantly faster than chemical mixing as the former process needs only a few, short-ranged atomic jumps, whereas the latter occurs by long-ranged diffusion. However, owing to the varying atomic mobility, details of the dissolution process depend on temperature. At 600 K, the thermal jump rate is still sufficient that the degree of order gets adapted to the local composition, driven by the potential $f(c,s)$. Hence disordering accelerates at the interfaces because of the reduced Al content inside the transition zone. In consequence, the continuum model can indeed describe a faster disordering of precipitates at these elevated temperatures owing to ion mixing at the interfaces.

By contrast, at room temperature, the thermal mobility is frozen as is demonstrated by a recent analysis of the reordering kinetics.[21] Since $L \approx M \approx 0$, Eqs. (3) and (4) get completely decoupled and composition and order develop independently from each other. Each precipitate disorders like homogeneous Ni_3Al, whereas the chemical dissolution proceeds very slowly on a different time scale. Thus, in the framework of the continuum model, the disordering rates of the decomposed alloy and Ni_3Al are predicted to be identical at room temperature, in obvious disagreement to the experimental observation.

In summary, we have to state that the continuum model reproduces characteristic features of the experiments at high temperatures, i.e., the establishment of a steady state with a much smaller degree of order in the decomposed systems. Minor discrepancies in the temperature scales are indicated by the very low order measured in the steady-state of homogeneous Ni_3Al at 550 °C, which should be, according to the model, already well above the critical temperature. But such quantitative disagreements are probably explained by the rough approximation of the thermodynamics or by an erroneously overestimated vacancy supersaturation. Very detailed variations of the composition profiles at the particle's interface, like the rather sharp compositional transitions predicted at 700 K compared to the smooth profiles at 600 K, could not be finally proven yet, owing to the limited accuracy of analysis.[29]

On the other hand, the model fails at room temperature even in a qualitative sense. Disordering and dissolution are described as purely ballistic processes, which do exchange atom positions randomly. Thus, when the system is no longer allowed to scan its configurational space by thermal jumps, any coupling between local order and composition vanishes in the modeling. As the frozen mobility at room temperature is proven by experiments, this shortcoming is a fundamental one, that cannot be overcome by a reasonable adjustment of the kinetic parameters or the free-energy representation. The deficit may only be eliminated, if the disordering efficiency ϵ in Eq. (4) is considered to be directly concentration dependent.

V. MONTE CARLO SIMULATION OF COLLISION CASCADES

How may a direct composition dependence of the disordering efficiency as indicated by the presented analysis be understood? Ballistic disordering by collision replacement sequences does not rely on the chemical nature of the replaced atoms so that any purely ballistic concept will certainly fail to explain such a composition dependence. However, in the case of ion irradiation, damage is predominantly generated inside localized collision cascades. During the late stages of so-called thermal spikes, when the average energy per atom falls below the order of 1 eV, the replacements will become sensitive to thermodynamics again. Within a small volume of a few nm diameter and during a very short period of a few tens of picoseconds, the system is able to sample various atomic configurations, although the average thermal mobility is virtually zero at room temperature.[21] Since the processes develop too fast to be investigated by experimental methods, the actual knowledge about cascade mechanisms relies mainly on computer simulations.[30] Molecular-dynamics (MD) studies (eg., Refs. 31 and 32) of ion irradiation in ordered Ni_3Al agree in so far that equivalent temperatures inside the spike core exceed the melting point of the material for a very short period of some picoseconds. The chemical order is largely suppressed in the *molten* core, but partly recovered during the later cooling stages. Thus, during the spike event, some reordering may take place[33] which is expected to depend on the composition inside the spike volume. In addition, it probably depends on the atomic configuration around the spike, which may become effective as a heterogeneous nucleation site for reordering.

In order to test this concept of a partly reordering statistically, a Monte Carlo (MC) simulation of the irradiation process was performed on a rigid lattice. The microstructural evolution considered in this paper is due to the collective result of many overlapping cascade events. Therefore the more strict treatment by a MD approach, which was very successful in elucidating the characteristics of isolated cascades, is still far beyond the actual computational possibilities. Instead we try to reproduce essential features of isolated events by a rather simple scheme and to predict the collective result of many overlapping cascades on the decomposed microstructure. The aim of the MC study is not to provide a detailed description of cascade events but to prove whether the concept of reordering yields a reasonable explanation of the observed faster disordering of precipitates.

In Fig. 9, the basic idea of our MC approach is illustrated. Cascade events are considered as well bounded spherical volumes of radius R. The site exchanges among the atoms caused by the ion impact are simulated by two different steps. First, all atoms inside a sphere of radius R are randomly exchanged [(a) ballistic mixing]. Subsequently, several vacancies are created inside the ballistically mixed volume by removing randomly selected atoms [(b) thermal spike]. The vacancies perform a diffusional walk at a constant relaxation temperature to imitate the cooling or relaxation stage of the spike. When they eventually reach a distance of $2R$ to the center of the event, the vacancies are

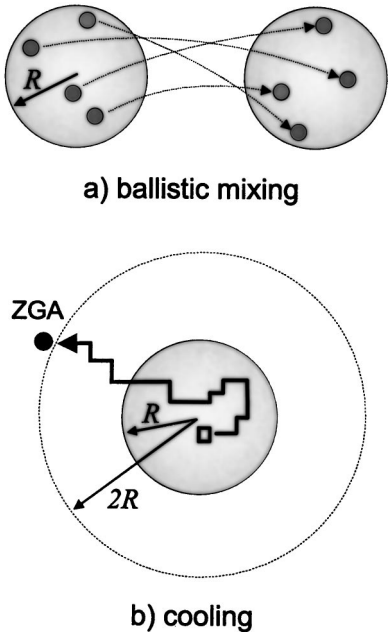

FIG. 9. Two-stage process to describe the mixing by cascade events.

annihilated by placing an Al or Ni atom, randomly chosen in accordance to the average alloy composition, at the vacant position. Outside the spike region the system is assumed to be frozen. The generation of vacancies close to the spike center and their annihilation by recombination with interstitials in an outer shell resembles the diluted central region and the compressed periphery of high interstitial density, which have been frequently observed in MD simulations. Nevertheless, it is important to note that the proposed reaction scheme assuming diffusion of isolated vacancies is only introduced to produce the atomic arrangement subsequent to the cascade event. The model is by no means suitable to simulate the real intracascade kinetics, which becomes particularly clear, when the diffusion time required by the generated vacancies to reach the annihilation zone is estimated. It exceeds the typical lifetime of a spike by one to two orders of magnitude, indicating that also the cooling stage of the spike represents a collective process rather than the migration of individual lattice defects.

Rhombohedrical volumes of 64^3 atoms and periodical boundary conditions are used for the simulation. Three different initial microstructures are considered (i) homogeneously ordered Ni_3Al, (ii) a spherical Ni_3Al precipitate of 5 nm radius, and (iii) eight smaller precipitates of 2.5 nm radius embedded in Ni matrix. With 6 at. %, the initial composition of the matrix was adjusted to the matrix solubility of the MC model at about 800 K. This way the total Al content of the simulated volume amounts to 9.3 at. % Al. The position of subsequent cascades are determined randomly with homogeneous probability. The diffusional walk of the relaxing vacancies is simulated obeying thermal statistics. For that, a vacancy jump model is used which has been recently reported to describe thermal reordering of disordered Ni_3Al.[21] Pair interactions between nearest and next-nearest neighbors are used to describe the energetics of the system.

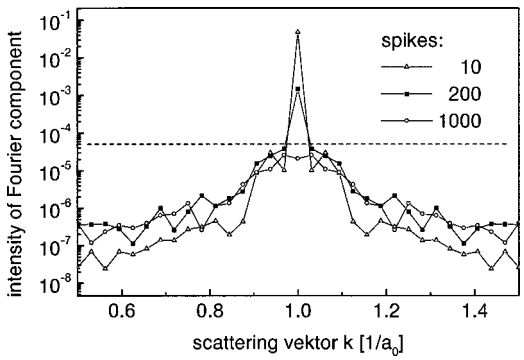

FIG. 10. MC simulation of the irradiation in homogeneous Ni_3Al at room temperature. Intensity profiles along [002] direction of the reciprocal lattice centered at $k_{[001]}$. Fluences are quantified by the number of spikes generated in the simulated volume.

Phase boundaries predicted by the MC model in thermal equilibrium are depicted in Fig. 6. Although the topology of the phase diagram is described correctly, the solubility of the Ni matrix is still underestimated, similar as for the continuum model discussed before. Beside to the phase equilibrium, the interaction parameters were also adjusted to the asymmetry of the vacancy energy on the Ni and Al sublattice of the ordered structure. This practice ensures that the ratio of the Ni and Al diffusion in the ordered structure is reproduced consistently with experimental data. This way, specific kinetic properties of the system are taken into account, which has been demonstrated in recent work by the simulation of thermal ordering.[21] Further technical details concerning the MC simulation of the vacancy jumps and quantitative interaction parameters are stated in this publication.

Important irradiation parameters of the MC model are the ballistic radius R, the number of vacancies n_{rel} generated inside the ballistic zone, and the relaxation temperature. The latter is kept constant at 1100 °C, as at this temperature the ordering efficiency of vacancy jumps is at maximum.[21] In MD calculations the radius of the *molten* zone was found to depend on the energy of the primary Ni ions according to[32]

$$R = 3a_0 E_{ion}^{1/3}. \tag{8}$$

A tendency to form subcascades is noticed in MD simulations already at ion energies above 5 keV, so that we certainly have to assume that several subcascades are formed per primary 300-keV Ni ions. Assuming the energy of an individual subcascade to be 10–20 keV, a radius of the *molten* zone of about 2.5 nm is quite reasonable. The number of generated vacancies is treated at first as a free parameter and will be discussed later.

By analogy to the experimental procedure, the LRO of the simulated structures is quantified by a Fourier transformation of the discrete distribution function

$$c(x_i) := \begin{cases} 1; & \text{if Al located at } x_i \\ 0; & \text{else.} \end{cases} \tag{9}$$

The intensity at the superlattice frequency $k_{[001]}$ is taken as a measure for LRO. In Fig. 10 linear intensity profiles through the reciprocal lattice are shown as obtained by a simulation

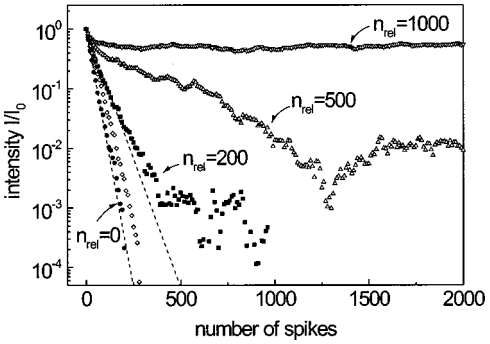

FIG. 11. Simulated disordering kinetics of homogeneous Ni_3Al for different reordering strengths ($n_{rel}=0$, 50, 200, 500, and 1000). The dashed lines represent exponential disordering with efficiencies $V_s/V=1/47$ and $V_s/V=1/94$.

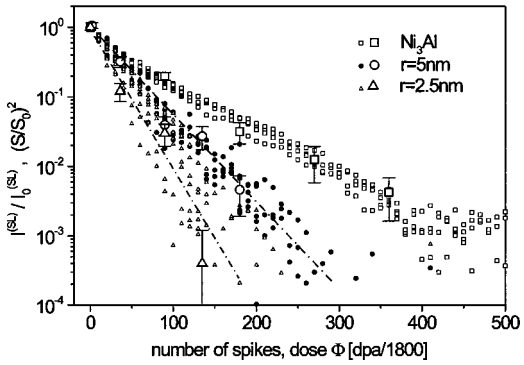

FIG. 12. Ion-induced disordering of stoichiometric Ni_3Al and two different decomposed microstructures (average composition Ni-9.3 at. %-Al). Comparison of MC simulation (small symbols) and experiment (large symbols). The dash-pointed regression lines indicate the average behavior of MC simulations for precipitates with 5 and 2.5 nm radius.

of the irradiation of homogeneous Ni_3Al with $n_{rel}=200$. After producing 200 spikes inside the simulated volume, the intensity has already decreased below 2% of the initial one. During further irradiation, a steady state of short-range order is established as indicated by the very broad intensity maximum developed at the superlattice position after performing 1000 spikes. The amount of this remaining order is controlled by the competition between cascade mixing and reordering. However, when comparing the simulation with the experiment, one must not neglect the finite sensitivity of the measurement which is realistically estimated to be about 1/1000 of the initial intensity. A dashed line in Fig. 10 indicates this limit, evidencing that the steady-state of the simulated structure would be characterized by the measurement as completely disordered.

If the simulated disordering kinetics of Ni_3Al is compared to the experimental result, an upper limit of the number of vacancies generated per spike may be determined. For that, the simulated disordering kinetics is shown for several different n_{rel} in Fig. 11. The experimental data revealed an exponential decay of LRO with increasing fluence. By simple geometric arguments an exponential decay is also expected for the MC data of purely ballistic mixing ($n_{rel}=0$). Assuming complete disordering inside the core volume, the fluence dependence of the LRO should be given by

$$s=\sqrt{\frac{I}{I_0}}=\exp(-n_s V_s/V), \tag{10}$$

where n_s, V_s, and V denote the number and core volume of performed spikes and the simulation volume, respectively. This is indeed obtained in the simulation as indicated by the left dashed line in Fig. 11 where $V_s/V=1/47$ according to the given geometrical situation. With increasing number of relaxing vacancies, disordering retards, the kinetics deviates from the former exponential behavior, and finally a finite steady-state degree of order is established, which becomes pretty clear for the case of $n_{rel}=1000$. However, the behavior obtained for a reordering strength of $n_{rel}=200$ is still consistent with the measurements, as significant deviations from the exponential decay are noticed in the simulations only at intensity ratios below 0.01, for which the experimental accuracy is already very weak. The initial disordering rate amounts to only half of that observed for purely ballistic disordering, which is seen by comparing the two dashed lines in the figure. Thus, with this reordering strength, the proposed spike model preserves a rest order of $s=0.5$ inside the core, if the spike is initiated in previously completely ordered Ni_3Al.

Applying the MC model to decomposed alloys, indeed a faster disordering of precipitates is predicted if the precipitate size is of the same order as the cascade size. Experimental results are compared with MC simulations in Fig. 12. Because of the heterogeneous nature of the cascade process, the simulated data show a strong statistical scattering. Results of four to eight statistically independent runs are shown in the figure. Dash-pointed lines indicate the average behavior of microstructures with precipitates of 5 and 2.5 nm radius. Nevertheless, the faster disordering of decomposed systems and the dependence on the particle size is clearly predicted and compared to the experimental data, the effect is found in the correct magnitude. For this comparison, the x axis of measurement and simulation have been calibrated to each other using the data of homogeneous Ni_3Al. We obtain the best matching between experiment and simulation for the already mentioned reordering strength of $n_{rel}=200$.

As the MC model is not constructed to describe the intracascade kinetics but to simulate the microstructural result after the cooling stage, there is no straightforward way to compare the model parameters with microscopic results of MD simulations. However, a study of cascade events in Ni_3Al with the latter method[34] revealed several tens of stable Frenkel defects in the final state and the maximum number of transient Frenkel pairs during the event is determined to 2500 for a cascade energy of 5 keV. These values indicate that $n_{rel}=200$ is quite a reasonable number for the relaxing vacancies in the MC model. In this context, it is remarkable that the rest order of $s=0.5$ predicted by the MC model agrees quite well with the value $s=0.6$ found in recent MD simulations of 10-keV cascades in Ni_3Al.[35] In spite of its simplicity, the MC model seems to describe some essential features of the cascade mixing and disordering realistically.

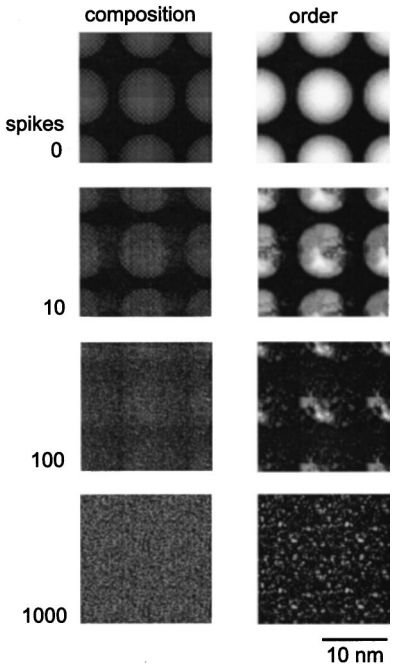

FIG. 13. Irradiation of an ordered precipitate (average composition of the simulated volume Ni-9.3 at. %-Al). Two-dimensional composition and order maps obtained by MC simulation. The local LRO shown in the right columns was determined at each lattice site evaluating the surrounding sites up to the fourth-neighbor shell.

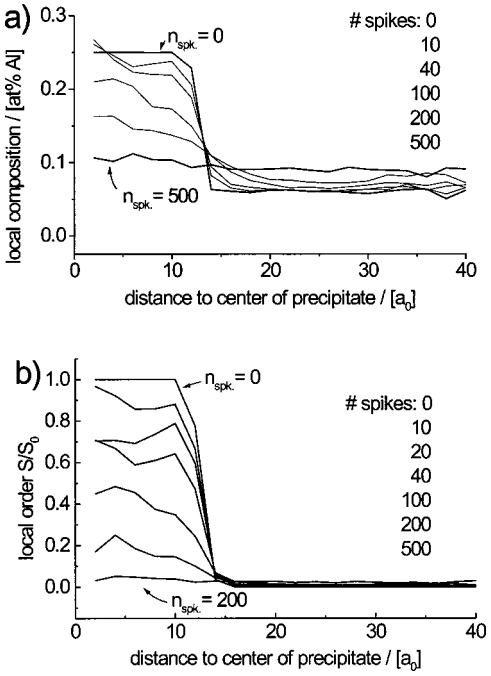

FIG. 14. Radial composition and order profiles determined at the precipitate shown in Fig. 13.

The heterogeneous nature of the cascade mixing becomes pretty clear by the two-dimensional composition and order maps shown in Fig. 13. To generate these maps, the simulated structure containing a precipitate of 5 nm radius has been projected along a [001] axis. The order maps in the right column compare to conventional dark field micrographs like those presented in Fig. 1, although the intensity scale is inverted and spread owing to the definition of the order parameter. As the size of precipitates and cascades are comparable, the disordering and dissolution of the precipitates proceed very inhomogeneously. Generating 100 spikes inside the simulation volume corresponds to a fluence of 0.055 dpa according to the calibration established in Fig. 12. The simulated morphology of the particle at this stage agrees pretty well with the experimental dark field image shown in Fig. 1(b), which was obtained at 0.05 dpa. Thus the assumed size of the cascade core seems to be quite reasonable. Through the simulated precipitate, radial profiles of local composition and order may be calculated similar as obtained by the continuum model (see Fig. 14). Comparing the MC result to the profiles of the continuum model at room temperature in Fig. 8, it becomes obvious that now the difference in dissolution and disordering rates is not that pronounced, which is due to the reordering inside the cascades. Disordering and mixing tend to be concomitant processes as they are strongly related inside the cascade core.

VI. DISCUSSION

Our experiments and their interpretation based on model calculations have shown that indeed information on the microscopic cascade process is obtained by a comparatively simple measurement of the average order parameter, if data of different microstructures are related to each other. We saw that the proposed continuum model describes the experiments at sufficiently high temperatures where, compared to the number of thermal jumps, the ballistic forcing results only in a small disturbance. By contrast, significant discrepancies are noticed at room temperature which, according to our present argument, cannot be avoided by a better adjustment of model parameters. To overcome the shortcoming a direct dependence of the disordering efficiency on the composition has been postulated. At this point one might ask whether this conclusion is really imperative. Are there other deficits of Eqs. (3) and (4), which might explain the observed discrepancy?

Martin pointed out that in general, kinetic field equations should contain cross terms coupling the driving force caused by a variation of order to the change of composition and vice versa,[36] similar as the representation of nonequilibrium thermodynamics introduced by Prigogine[37] connects each driving force to the current of each species by a general mobility matrix. These cross terms have been neglected in our equations without a sounded justification. Furthermore, the Gibbs free energy determined as an equilibrium potential will become increasingly erroneous with increasing deviation from equilibrium conditions. However, all these objections become irrelevant if the thermal mobility, i.e., the number of atomic jumps outside cascade events, vanishes. Since irradiated specimens show no tendency of relaxation even after several months of room-temperature storage,[21] obviously the thermal mobility is frozen at room temperature. The insignificance of thermal jumps is further proved by the fact that the observed disordering kinetics is independent of the dose rate when plotted versus the accumulated dose. Thus we be-

lieve that a direct composition dependence of the disordering efficiency in the case of heavy-ion irradiation is evident.

As a stochastic model, the MC simulations do not suffer from an inappropriate equilibrium potential. However, although performing a statistical correct treatment, the MC model will yield wrong results if the assumed microscopic process is inappropriate. Regarding this aspect, our model certainly needs considerable refining in order to obtain a real quantitative description. As an Ansatz to improve the microscopic model, the relation between the disordering and mixing efficiencies may be compared with experimental values. Neglecting the reordering step, the MC model yields by geometric considerations

$$\epsilon\Phi = n_c V_c, \tag{11}$$

and

$$\kappa\Phi = \frac{n_c V_c \overline{L^2}}{6}, \tag{12}$$

where n_c, V_c, and $\overline{L^2}$ denote the number of generated cascades per volume, the volume of the cascade core, and the average square jump distance of an atom inside the core, respectively. Assuming a random redistribution of all atoms inside the spherical core, we have

$$\overline{L^2} = \frac{6}{5} R^2, \tag{13}$$

so that the ratio of the mixing and disordering efficiencies is geometrically fixed in our simple cascade core model to

$$\frac{\kappa}{\epsilon} = \frac{R^2}{5}. \tag{14}$$

Obviously, the size of the cascade core is severely limited by this relation if realistic ratios between mixing and disordering should be established. Regarding this relation, the core size used in our simulation is chosen at maximum. More complex models of the cascade process must be used to overcome this limitation, as has been already proposed by Turkin *et al.*[38] They subdivide the cascade volume into a core region, where the atoms are randomly redistributed to an outer shell where complete disordering takes place but only a very limited jump distance of the atoms is assumed. However, their model is a purely ballistic one. No influence of thermodynamics is taken into account, so that it is inappropriate to explain our experiments.

According to the simulation, the dynamic reordering inside the cascade core should result in deviations from an exponential disordering kinetics, which could not be proven by our experiments because of the limited measurement accuracy. To study these effects, more accurate measurements are suggested, which might be achieved by dedicated detector systems or imaging plates. This way, the evaluation of micrographs of a very limited dynamical range becomes obsolete. By Müller[39] measurements of the disordering of homogeneous Ni_3Al were performed utilizing imaging plates, which indeed indicate a very weak tendency of reordering. Unfortunately, he followed an isochronous instead of isothermal measurement scheme, so that the kinetic behavior cannot be followed in detail.

VII. CONCLUSION

The ion induced disordering of decomposed NiAl alloys was studied by quantitative electron diffractometry. The experimental results were compared to predictions obtained by an analytical continuum model and Monte Carlo simulations.

At room temperature, the experiments revealed an exponential disordering kinetics for homogeneous Ni_3Al as well as small Ni_3Al precipitates. It is proven by a direct comparison of the data that decomposed systems disorder about two times faster than the homogeneous one. Furthermore, the disordering rate increases with decreasing particle size. Disordering gets retarded at elevated irradiation temperatures, and at 550 °C a steady state is established. Compared to their respective values before irradiation, the steady-state degree of LRO in the decomposed specimen is significantly smaller than that of homogeneous Ni_3Al.

Describing the kinetics by a continuum model, it is shown that the smaller steady-state degree of LRO in the decomposed system is due to an irradiation enhanced Al solubility of the matrix. Further evidence for this interpretation follows from the experimental size distributions of the precipitates. In the steady state, precipitates are considerably shrunk compared to the initial microstructure.

The continuum model fails to describe the experimental observations at room temperature which is caused by the exclusively ballistic ansatz used to describe the ion mixing and disordering. Monte Carlo simulations, which model thermodynamic effects inside the cascade core, demonstrate that dynamical reordering inside the cascade core must be taken into account to understand the room-temperature experiments. Thus our experiments confirm the importance of the thermal spike concept in order to understand ion induced mixing.

The MC simulations suggest that the simple exponential disordering kinetics observed in the experiment at room temperature is an artifact of the limited measurement accuracy. More exact measurements of the superlattice reflection variation with irradiation time should reveal very small finite rest orders in the range of 0.1–1% and the retardation of disordering to intermediate fluences.

ACKNOWLEDGMENTS

The authors are grateful to C. Abromeit of the Hahn Meitner Institut in Berlin for many valuable discussions. Financial support by the Deutsche Forschungsgemeinschaft (SFB 345) is gratefully acknowledged.

APPENDIX: KINETIC COEFFICIENTS OF DIFFUSION AND ORDERING

As aforementioned, the mobility coefficients in the evolutionary Eqs. (3) and (4) for long-range transport and ordering are not independent, since both processes are based on the same microscopic mechanism, i.e., the site exchange be-

tween atom and vacancy. In order to properly connect the time scales, the relation between M and L is determined by a mean-field consideration assuming the same level of approximation which has been used to obtain the evolutionary equations.

The sublattice structure of the $L1_2$ order suggests to subdivide the Gibbs free energy into four partial energies taking into account the chemical potentials of both atom types on the different sublattice sites, according to

$$f=\frac{N}{4}[c_\alpha\mu_{Al}^{\alpha}+(1-c_\alpha)\mu_{Ni}^{\alpha}+3c_\beta\mu_{Al}^{\beta}+3(1-c_\beta)\mu_{Ni}^{\beta}], \tag{A1}$$

where α denotes the corner sublattice of the ordered structure and β the three sublattices of face-centered sites which are identically occupied in the case of $L1_2$ order. In addition we have

$$\mu_{Al}^{j}=E_{Al}^{j}+kT\ln c_j;\quad \mu_{Ni}^{j}=E_{Ni}^{j}+kT\ln(1-c_j). \tag{A2}$$

The atoms are performing thermal activated jumps in random directions with a jump frequency determined by the energy of a particular site, so that

$$\nu=\nu_0\exp\left[\frac{E_k^j}{kT}\right], \tag{A3}$$

with a suitable chosen vibration frequency. Thus the number of Al atoms jumping away from the corner sublattice per time is given by

$$\frac{\overrightarrow{dN_{Al}^{\alpha}}}{dt}=\frac{N}{4}\nu_0 c\frac{c_\alpha}{c}\exp\left[\frac{E_{Al}^{\alpha}}{kT}\right]=\frac{N}{4}\nu_0 c\exp\left[\frac{E_{Al}^{\alpha}+kT\ln(c_\alpha/c)}{kT}\right]. \tag{A4}$$

Similar rate equations hold for the three other combinations of atom and sublattice types. The total change rate of the Al atoms on the α sublattice is then obtained by the balance of jumps away from and towards the sublattice where one has to take into account that only a third of the jumps from the three β lattices are directed towards the α lattice, which yields

$$\frac{dN_{Al}^{\alpha}}{dt}=-\frac{\overrightarrow{dN_{Al}^{\alpha}}}{dt}+\frac{\overrightarrow{dN_{Al}^{\beta}}}{dt} \tag{A5}$$

$$=\frac{N}{4}\nu_0 c\left\{\exp\left[\frac{E_{Al}^{\beta}+kT\ln(c_\beta/c)}{kT}\right]-\exp\left[\frac{E_{Al}^{\alpha}+kT\ln(c_\alpha/c)}{kT}\right]\right\} \tag{A6}$$

$$\approx\frac{N}{4}\frac{\nu_0 c}{kT}\{\mu_{Al}^{\beta}-\mu_{Al}^{\alpha}\}. \tag{A7}$$

The linearization of the exponential functions required to obtain the last expression is at least justified for small order degrees where the actual concentration on the sublattice c_α is only slightly different from the average composition c. Performing the same calculation for the Ni atoms on the α sublattice,

$$\frac{dN_{Ni}^{\alpha}}{dt}\approx\frac{N}{4}\frac{\nu_0(1-c)}{kT}\{\mu_{Ni}^{\beta}-\mu_{Ni}^{\alpha}\} \tag{A8}$$

is obtained. Combining the definition of the LRO parameter [Eq. (2)] with Eqs. (A7) and (A8), the time variation of the order parameter follows with a few lines of calculation:

$$\frac{ds}{dt}=\frac{\partial s}{\partial c_\alpha}\cdot\frac{\partial c_\alpha}{\partial t} \tag{A9}$$

$$=\frac{1}{3c}\frac{4}{N}\left((1-c_\alpha)\cdot\frac{dN_{Al}^{\alpha}}{dt}-c_\alpha\cdot\frac{dN_{Ni}^{\alpha}}{dt}\right) \tag{A10}$$

$$=\frac{1}{3c}\cdot\frac{c(1-c)\nu_0}{kT}\cdot(\mu_{Al}^{\beta}-\mu_{Al}^{\alpha}-\mu_{Ni}^{\beta}+\mu_{Ni}^{\alpha}), \tag{A11}$$

where the number of Al and Ni atoms have to be varied independently because of the vacancy mechanism and $c_\alpha\approx c$ is tacitly assumed. If the sublattice compositions in Eq. (A1) are expressed by the order parameter using Eq. (2), the variation of free energy [Eq. (A1)] with long-range order is calculated to

$$\frac{\partial f}{\partial s}=\frac{3c}{4}(-\mu_{Al}^{\beta}+\mu_{Al}^{\alpha}+\mu_{Ni}^{\beta}-\mu_{Ni}^{\alpha}), \tag{A12}$$

which allows to transform Eq. (A11) into

$$\frac{\partial s}{\partial t}=-\underbrace{\frac{4}{9c^2}\cdot\frac{c(1-c)\nu_0}{kT}}_{:=M}\cdot\frac{\partial f}{\partial s}. \tag{A13}$$

Comparing this expression to Eq. (4), the mobility coefficient is identified. Finally, M is related to L regarding the definition of the transport mobility

$$L=\frac{\nu_0\lambda^2}{6}\cdot\frac{c(1-c)}{kT} \tag{A14}$$

(λ denotes the next-neighbor jump distance) by

$$M=\frac{8}{3}\cdot\frac{1}{c^2\lambda^2}\cdot L=\frac{16}{3}\cdot\frac{1}{c^2a_0^2}\cdot L, \tag{A15}$$

which was used to integrate the evolutionary equations as stated in Sec. IV.

*Corresponding author. Electronic address: guido@umpa03.gwdg.de

[1] K. Russel, Prog. Mater. Sci. **28**, 229 (1984).
[2] P. Bellon and G. Martin, Phys. Rev. B **39**, 2403 (1989).
[3] F. Haider, P. Bellon, and G. Martin, Phys. Rev. B **42**, 8274 (1990).
[4] R.S. Nelson, J.A. Hudson, and D.J. Mazey, J. Nucl. Mater. **44**, 318 (1972).
[5] G. Martin, F. Soisson, and P. Bellon, J. Nucl. Mater. **205**, 301 (1993).
[6] A. Yavari, Acta Metall. Mater. **41**, 1391 (1993).
[7] M.D. Baro, Acta Metall. Mater. **41**, 1065 (1993).
[8] F. Cardellini, J. Mater. Res. **8**, 2504 (1993).
[9] P. Scherrer, C. Dimitropoulos, F. Borsa, and S. Rubini, Phys. Rev. B **57**, 10 462 (1998).
[10] G. Carpenter and E. Schulson, Scr. Metall. **15**, 549 (1981).
[11] H. Liu and T. Mitchell, Acta Metall. **31**, 863 (1983).
[12] O. Dimitrov and C. Dimitrov, Intermetallics **2**, 249 (1994).
[13] C. Abromeit, S. Mueller, and N. Wanderka, Scr. Metall. **32**, 1519 (1995).
[14] S. Mueller, M.L. Jenkins, C. Abromeit, and H. Wollenberger, Philos. Mag. **75**, 1625 (1997).
[15] J. Ziegler, J. Biersack, and V. Littmark, *The Stopping and Range of Ions in Solids* (Pergamon, New York, 1985).
[16] V. Naundorf, M.-P. Macht, and H. Wollenberger, J. Nucl. Mater. **186**, 227 (1992).
[17] E. Camus, C. Abromeit, F. Bourdeau, N. Wanderka, and H. Wollenberger, Phys. Rev. B **54**, 3142 (1996).
[18] F. Bourdeau, E. Camus, C. Abromeit, and H. Wollenberger, Phys. Rev. B **50**, 16 205 (1994).
[19] II. Physikalische Institut, Universität Göttingen.
[20] M. Uhrmacher, K. Pampus, F.J. Bergmeister, D. Purschke, and K. Lieb, Nucl. Instrum. Methods Phys. Res. B **9**, 234 (1985).
[21] J.C. Ewert and G. Schmitz, Eur. Phys. J. B **17**, 391 (2000).
[22] J.C. Ewert, G. Schmitz, F. Harbsmeier, M. Uhrmacher, and F. Haider, Appl. Phys. Lett. **73**, 3363 (1998).
[23] G. Martin, Phys. Rev. B **30**, 1424 (1984).
[24] S. Matsumura, S. Müller, and C. Abromeit, Phys. Rev. B **54**, 6184 (1996).
[25] R. Sizman, J. Nucl. Mater. **69**, 386 (1978).
[26] J. C. Ewert, Ph.D. thesis, University of Göttingen, 1998.
[27] A.G. Khachaturyan, T.F. Lindsey, and J.W. Morris, Metall. Trans. A **19**, 249 (1988).
[28] A.J. Ardell, Acta Metall. **16**, 511 (1968).
[29] C. Abromeit, E. Camus, and S. Matsumura, J. Nucl. Mater. **271&272**, 246 (1999).
[30] R.S. Averback, J. Nucl. Mater. **216**, 49 (1994).
[31] T. Diaz de la Rubia, A. Caro, and M. Spaczer, Phys. Rev. B **47**, 11 483 (1993).
[32] F. Gao and D.J. Bacon, Philos. Mag. A **71**, 65 (1995).
[33] C. Abromeit and H. Wollenberger, J. Nucl. Mater. **191-194**, 1092 (1992).
[34] F. Gao and D.J. Bacon, Philos. Mag. A **71**, 43 (1995).
[35] F. Gao and D.J. Bacon, in *Microstructural Processes in Infrared Materials*, edited by S. J. Zinkle *et al.*, MRS Symposia Proceedings No. 540 (Materials Research Society, Pittsburgh, 1999), p. 661.
[36] G. Martin, Phys. Rev. B **50**, 12 362 (1994).
[37] I. Prigogine, *Introduction to Thermodynamics of Irreversible Processes* (Interscience Publications, New York, 1968).
[38] A.A. Turkin, C. Abromeit, and V. Naundorf, J. Nucl. Mater. **233-237**, 979 (1996).
[39] S. Müller, Ph.D. thesis, Techn. Univ., Berlin, 1997.
[40] A.J. Ardell, R.B. Nicholson, and J.D. Eshelby, Acta Metall. **14**, 1295 (1966).